

Development

# Development of the Functional Connectome Topology in Adolescence: Evidence from Topological Data Analysis

Zeus Gracia-Tabuenca,<sup>1</sup> Juan Carlos Díaz-Patiño,<sup>1,2</sup> Isaac Arelio-Ríos,<sup>1</sup>  
Martha Beatriz Moreno-García,<sup>1</sup> Fernando A. Barrios,<sup>1</sup> and Sarael Alcauter<sup>1</sup>

<https://doi.org/10.1523/ENEURO.0296-21.2022>

<sup>1</sup>Instituto de Neurobiología, Universidad Nacional Autónoma de México, Querétaro 76230, México and <sup>2</sup>Centro de Investigación Científica y de Educación Superior de Ensenada, Ensenada 22860, México

## Abstract

Adolescence is a crucial developmental period in terms of behavior and mental health. Therefore, understanding how the brain develops during this stage is a fundamental challenge for neuroscience. Recent studies have modeled the brain as a network or connectome, mainly applying measures from graph theory, showing a change in its functional organization, such as an increase in its segregation and integration. Topological Data Analysis (TDA) complements such modeling by extracting high-dimensional features across the whole range of connectivity values instead of exploring a fixed set of connections. This study inquires into the developmental trajectories of such properties using a longitudinal sample of typically developing human participants ( $N = 98$ ; 53/45 female/male; 6.7–18.1 years), applying TDA to their functional connectomes. In addition, we explore the effect of puberty on individual developmental trajectories. Results showed that the adolescent brain has a more distributed topology structure compared with random networks but is more densely connected at the local level. Furthermore, developmental effects showed nonlinear trajectories for the topology of the whole brain and fronto-parietal networks, with an inflection point and increasing trajectories after puberty onset. These results add to the insights into the development of the functional organization of the adolescent brain.

**Key words:** adolescence; functional connectivity; persistence homology; puberty; resting state functional magnetic resonance imaging; topological data analysis

## Significance Statement

Topological Data Analysis (TDA) may be used to explore the topology of the brain along the whole range of connectivity values instead of selecting only a fixed set of connectivity thresholds. Here, we explored some properties of the topology of the brain's functional connectome and how they develop in adolescence. We show that developmental trajectories are nonlinear and better adjusted by puberty status than chronological age, with an inflection point around the onset of puberty. In particular, the results show that the topology of the fronto-parietal network is the one that drives the functional connectome changes in the adolescent period.

## Introduction

Adolescence is a critical development period that substantially impacts the body and behavior. Notably, the brain undergoes structural and functional changes

influenced by pubertal hormones (Vijayakumar et al., 2018; Laube et al., 2020). Moreover, these changes occur along with a consolidation of cognitive and

Received July 10, 2021; accepted December 1, 2022; First published January 30, 2023.

The authors declare no competing financial interests.

Author contributions: Z.G.-T., J.C.D.-P., I.A.-R., M.B.M.-G., F.A.B., and S.A. designed research; Z.G.-T., M.B.M.-G., F.A.B., and S.A. performed research; Z.G.-T. and J.C.D.-P. analyzed data; Z.G.-T., J.C.D.-P., I.A.-R., and S.A. wrote the paper.

executive performance (Baum et al., 2017; Chai et al., 2017).

These insights have been addressed by modeling the brain as a complex network of interacting nodes at task or rest conditions (Biswal et al., 1995; Smith et al., 2009). In this framework, the functional connectome is described by its system properties in biologically plausible terms, mainly using measures from graph theory (Rubinov and Sporns, 2010). Although graph metrics provide an effective framework to describe brain organization properties, they also have some limitations. The main limitation is that graph theory relies on pairwise connections as the basic unit of the network; in this regard high-order interactions within the network cannot be properly handled (Lord et al., 2016). Another potential limitation is the common step of thresholding, which is to discard a subset of the network connections based on several criteria (e.g., statistically, low values, sign, etc.). There is no consensus about this step, and functional connectomes tend to be unstable at different thresholds (Garrison et al., 2015), although group inferences may dramatically change based on thresholding (Gracia-Tabuenca et al., 2020). Nevertheless, other methods have recently been applied to address high-dimensional data, such as Topological Data Analysis (TDA; Sizemore et al., 2018; Expert et al., 2019). TDA models the connectome as a topological space and characterizes its interaction patterns as geometric features, allowing it to simplify complex structures at different scales (Giusti et al., 2015; Santos et al., 2019; Centeno et al., 2022). In particular, TDA applied to functional connectomes is not affected by the potential biases of connectivity thresholding nor brain segmentation (H. Lee et al., 2012; Gracia-Tabuenca et al., 2020); additionally, TDA is a suitable tool to address longitudinal data since it can extract invariant topological features into longitudinal designs (Fülöp et al., 2020). This methodology has been used for over a decade in neuroimaging (Chung et al. 2009; H. Lee et al., 2011, 2012, 2019;

This work was supported by the Consejo Nacional de Ciencia y Tecnología (CONACYT) Fellowship 330142 (to Z.G.-T.) for being a doctoral student of Programa de Doctorado en Ciencias Biomédicas, Universidad Nacional Autónoma de México (UNAM), a Universidad Nacional Autónoma de México-Dirección General de Asuntos del Personal Académico (UNAM-DGAPA) postdoctoral fellowship, and UNAM-Programa de Apoyo a Proyectos de Investigación e Innovación Tecnológica (UNAM-PAPIIT) Grants IN208622 and IN212219 (to S.A.).

**Acknowledgments:** We are incredibly grateful to the children and parents who participated in this study voluntarily. We thank Nuri Aranda López, Leonor Casanova Rico, César Arturo Domínguez Frausto, Deisy Gasca Martínez, Leopoldo González Santos, Ma. de Lourdes Lara Ayala, Juan J. Ortiz, and Erick H. Pasaye for their technical support. We also thank Rafael Fajardo, Roberto E. Mercadillo, and Edna Navarrete for their support in the psychological assessment and Michael C. Jeziorski for editing this manuscript. We thankfully acknowledge the imaging resources and support provided by the Laboratorio Nacional de Imagenología por Resonancia Magnética, Consejo Nacional de Ciencia y Tecnología (CONACYT) network of national laboratories.

Correspondence should be addressed to Sarael Alcauter at [alcauter@inb.unam.mx](mailto:alcauter@inb.unam.mx).

<https://doi.org/10.1523/ENEURO.0296-21.2022>

Copyright © 2023 Gracia-Tabuenca et al.

This is an open-access article distributed under the terms of the [Creative Commons Attribution 4.0 International license](https://creativecommons.org/licenses/by/4.0/), which permits unrestricted use, distribution and reproduction in any medium provided that the original work is properly attributed.

Choi et al., 2014; M.H. Lee et al., 2015; Chung et al., 2019) but is not the standard procedure in neuroimaging. Furthermore, it explores different properties to those explored with graph theory or other network approaches that typically explore the fully connected network [when only one single component is present, i.e., when  $Betti-0 (B_0) = 1$ ].

In terms of the functional organization of the brain, previous cross-sectional studies have shown that the adolescent period is characterized by an increase in modularity and specialization (Fair et al., 2009; Satterthwaite et al., 2013a; Gu et al., 2015), with prominent effects in frontal and parietal systems, along with executive performance (Marek et al., 2015; Gracia-Tabuenca et al., 2021). However, as far as we are concerned, TDA in human connectomes has mainly been applied to neuropsychiatric disorders (H. Lee et al., 2012, 2017; Gracia-Tabuenca et al., 2020; Li et al., 2021) but not to characterize the typical development. There is still a huge degree of uncertainty in this field because of the great variability between samples, sexes, and cultures (Sawyer et al., 2018), with special emphasis on the fact that some individuals have faster or slower pubertal development even when they have the same chronological age (Blakemore et al., 2010; Vijayakumar et al., 2018). In this regard, longitudinal trajectories and pubertal markers are highly valuable in describing adolescent development.

Therefore, this study focuses on how the topology structure of the neurotypical functional connectome changes during the adolescent period. In order to achieve that, TDA features were extracted from the functional brain connectivity of a longitudinal sample of typically developing subjects, and (non)linear trends were tested from chronological age and pubertal status.

## Materials and Methods

### Sample

A general invitation was sent to local schools describing the study protocols and the inclusion/exclusion criteria. Inclusion criteria consisted of a full-term gestation ( $\geq 37$  weeks). Exclusion criteria included academic year repetition and any neurologic or psychiatric disorder identified with the MINI semi-structured interview. Signed informed consent for parents and verbal assent for minors was required. The study protocols followed the ethical principles of the Declaration of Helsinki and were approved by the Institutional Ethics Board.

The sample comprised 98 typically developing participants (53 females, 45 males; age range: 6.7–18.1 years old). Of those, 41 returned for a second session, and 16 for a third. Initially, the study was designed as a cross-sectional study. However, to include intraindividual development in the growth charts, some participants agreed to participate in one or two follow-up sessions. As a result, follow-ups occurred after five years and the second after two years, respectively (Fig. 1).

### Pubertal status assessment

Participants fulfilled the Pubertal Development Scale (PDS; Petersen et al., 1988). PDS averages the response of five self-reported questions about growth spurt in

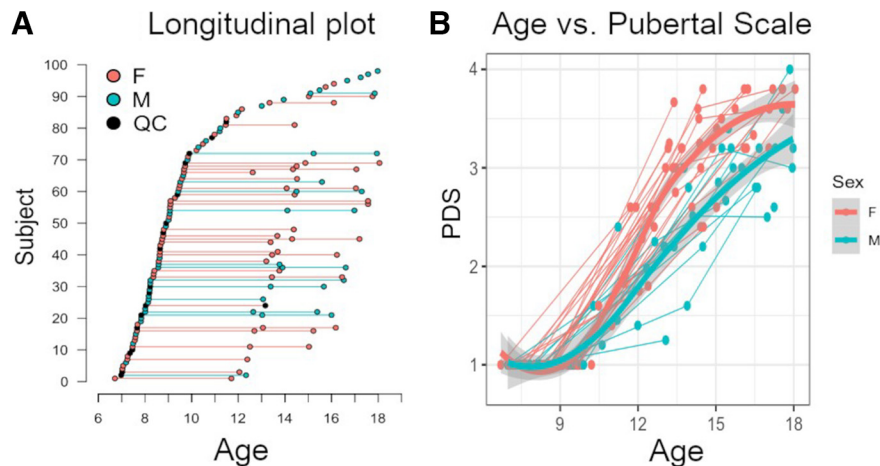


**Figure 1.** **A**, Longitudinal plot: each dot represents a subject at the age of assessment. Lines represent longitudinal assessments of a subject. **B**, Pubertal Development Scale scores (PDS) along age. Thin lines represent individual trajectories; thick lines represent locally estimated scatterplot smoothing (LOESS) curves per sex group (with 95% confidence-interval shadow) after controlling for intraindividual trends. F, female; M, male; QC, session with excessive motion artifact. Figures were modified from Gracia-Tabuenca et al. (2021) under CC BY 4.0 license (<https://creativecommons.org/licenses/by/4.0/>).

height, pubic hair, and skin change for both sexes; plus breast growth and menarche for females and facial hair growth and voice change for males. Responses are absence (1), first signs (2), evident (3), and finished (4) pubertal spurt. Those participants under 10 years old were set to PDS level 1, following similar values in previous studies (Hibberd et al., 2015; van Duijvenvoorde et al., 2019). In addition, 8 missing values (four females) were estimated via generalized additive mixed model (GAMM) with age-sex interaction locally estimated scatterplot smoothing (LOESS) curves (according to Gracia-Tabuenca et al., 2021).

### Imaging

Participants underwent a magnetic resonance imaging (MRI) protocol for each session, including a whole-brain functional MRI (fMRI) sequence plus high-resolution T1-weighted images for anatomic reference. After five “dummy” volumes for scan stabilization, a total of 150 fMRI volumes were obtained using a gradient recalled T2\* echoplanar imaging sequence (TR/TE=2000/40 ms, voxel size  $4 \times 4 \times 4$  mm<sup>3</sup>). Participants were instructed to lay down, close their eyes, and not fall asleep. In order to ease participants to remain awake, the fMRI scan was applied at the beginning of the MRI session and always in the morning. T1 images were obtained using a 3D spoiled gradient recalled (SPGR) acquisition (TR/TE = 8.1/3.2 ms, flip angle = 12.0, voxel size  $1 \times 1 \times 1$  mm<sup>3</sup>). All brain imaging was acquired with a 3T MR GE750 Discovery scanner (General Electric) using an 8-channel-array head coil. However, 20 sessions were acquired with a 32-channel coil; thus, a covariate was included in the subsequent analyses.

### Preprocessing

Structural T1 volumes were denoised with nonlocal means (Manjón et al., 2010) and N4 bias field correction (Tustison et al., 2010). fMRI datasets were preprocessed

using FSL v.5.0.6 (Jenkinson et al., 2012; RRID:SCR\_002823). Preprocessing steps included slice timing, head motion correction, brain extraction, intensity normalization, confound regression, spatial normalization, and 0.01- to 0.08-Hz bandpass filtering.

Considering that the pediatric population tends to move more inside the scanner (Satterthwaite et al., 2012), we implemented a strident strategy of confounding variables regression (Satterthwaite et al., 2013b). A total of 36 parameters were regressed out from the fMRI time series, including the six head-motion estimated parameters plus the average time series of the global signal, white matter, and cerebrospinal fluid. The derivatives of these nine variables were also added, and the quadratic terms of those eighteen. Additionally, the volumes with a framewise displacement (FD-RMS; Jenkinson et al., 2002)  $>0.25$  mm (“spikes”) were included as confounds as well. This approach overpowers other widely used motion-mitigation methods (Ciric et al., 2017; Parkes et al., 2018; Taymourtash et al., 2019; Graff et al., 2022). Eighteen sessions with  $<4$  min without spike-volumes were discarded (Satterthwaite et al., 2013b; Parkes et al., 2018); therefore, the final sample consisted of 89 participants (39 male, age range: 6.7–18.1 years old), of whom 37 and 11 had two and three longitudinal sessions, respectively.

In addition, fMRI datasets were co-registered to their T1 volume with six degrees of freedom and then warped twice using nonlinear SyN transformation (Avants et al., 2008; RRID:SCR\_004757) to a pediatric template (NIHPD4.5–18.5; Fonov et al., 2011) and then to the MNI-152 standard template.

### Functional connectomes

Brain networks were defined based on 264 regions of interest (ROIs) as nodes (Power et al., 2011). Pairwise edges were calculated through Pearson’s correlation between the average fMRI preprocessed signal of every pair of ROIs.

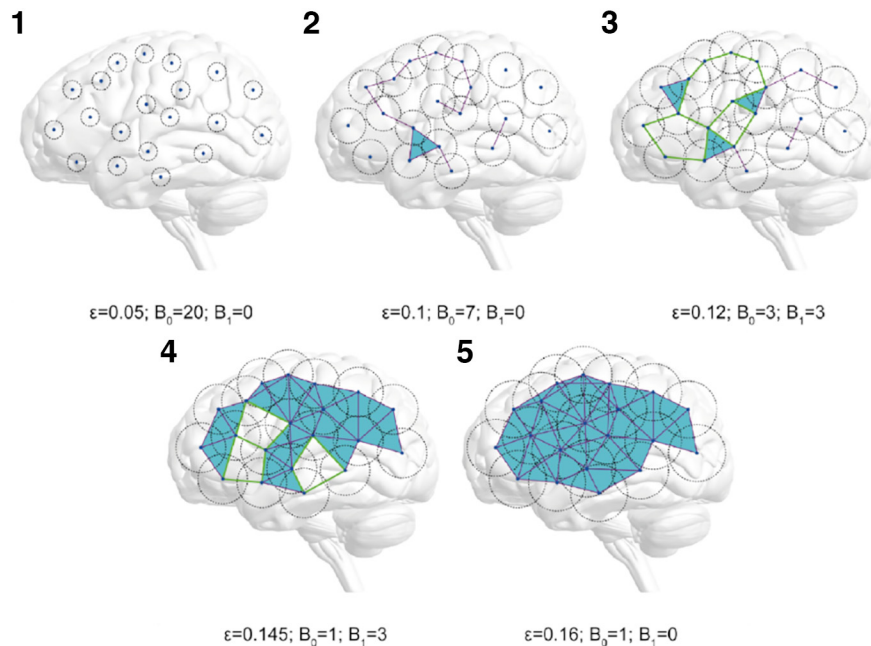


**Figure 2.** Betti-0 ( $B_0$ ) and Betti-1 ( $B_1$ ) for different filtration values. Illustrative example with 20 nodes, five filtration values  $\varepsilon$ , represented as the circle diameter and their corresponding  $B_0$  and  $B_1$  values. At  $\varepsilon = 0$ , the number of components ( $B_0$ ) equals the number of nodes, and there are no holes. As the filtration value increases, the number of components ( $B_0$ ) decreases until they form a single component containing all the nodes. Meanwhile, the number of holes ( $B_1$ ) starts at 0, increases, and finally goes back to 0 again. A hole of dimension 1 is a cycle with four or more edges (highlighted with green edges); the simplices of dimension  $>1$  are colored in light blue for each filtration value  $\varepsilon$ .

These ROIs consist of 5-mm radius spheres with high consistency in task and rest tested in large fMRI databases (Power et al., 2011). Moreover, this set of ROIs can be grouped in thirteen functional networks. This segmentation has been applied in numerous pediatric studies (Satterthwaite et al., 2013a; Gu et al., 2015; Marek et al., 2015; Chai et al., 2017; Ciric et al., 2017; Gracia-Tabuenca et al., 2020, 2021).

### Topological data analysis

The functional connectome can be modeled as a topological space using the Rips complex, defined as  $Rips(F, \varepsilon)$ .  $F$  stands for the set of nodes (same as the connectome nodes), and  $\varepsilon$  stands for the filtration value that indicates if a pair of nodes of  $F$  are connected (those with a distance lower than  $\varepsilon$ , see below the definition of distance). Thus, the set of connected nodes of the Rips complex varies as a function of  $\varepsilon$ . Additionally, topological features can be extracted from the Rips complexes, the so-called Betti numbers. Specifically, Betti numbers of order zero or Betti-0 ( $B_0$ ) accounts for the number of components (i.e., the number of groups of connected nodes and isolated nodes), Betti-1 ( $B_1$ ) accounts for the number of 1-dimensional holes which correspond to cycles in the network (Fig. 2), and so on (for an extensive review on TDA, we suggest Sizemore et al., 2019; Edelsbrunner and Harer, 2010).

In this study, we focused exclusively on  $B_0$  and  $B_1$ . When  $\varepsilon = 0$ ,  $B_0$  equals the number of nodes. As  $\varepsilon$  increases,  $B_0$  decreases and eventually will reach a single

component where every node of  $F$  is connected (Fig. 2). In contrast, at low values of  $\varepsilon$ , there are no holes in the connected pattern of the topological space because there are not enough connections to build them. Similarly, at high values of  $\varepsilon$ , the holes are “filled” because all pairwise connections within the component are accomplished. These holes represent serially distributed connections of nodes without shortcuts, while a filled hole means that those nodes are densely connected between them (Sizemore et al., 2018). Therefore, the greater amount of holes (i.e.,  $B_1$ ) is reached at intermediate values of  $\varepsilon$ . Both processes can be characterized as Betti curves as a function of  $\varepsilon$  (Fig. 3).

The distance between nodes was set as one minus their corresponding Pearson’s correlation (i.e., their functional connectivity edge), following H. Lee et al. (2012):  $d(\xi, x_j) = 1 - r(\xi, x_j)$ ,  $r$  being the Pearson’s correlation between nodes  $\xi$  and  $x_j$ .  $B_0$  and  $B_1$  curves were computed using the TDA R-package (Fasy et al., 2014), and were summarized employing the area under the curve (AUC). This metric, also known as a Persistence Indicator Function and Total Persistence, is a norm associated with the persistence diagrams (Rieck et al., 2020). In addition, stability properties have been proved (Cohen-Steiner et al., 2010), and; it also has been used for the classification of subjects in fMRI datasets (Caputi et al., 2021). The AUC accounts for the overall process of the Betti numbers along all possible values of  $\varepsilon$ . Low scores of  $B_0$ -AUC can be interpreted as a fast transition to the single component. In contrast, higher scores imply a more distributed configuration of the nodes that impedes a rapid transition



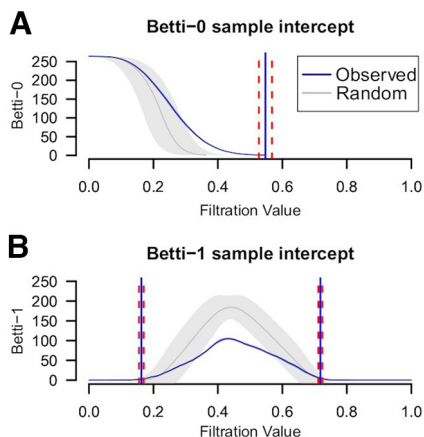


**Figure 3.** Sample intercepts for the  $B_0$  (A) and  $B_1$  (B) curves are in blue. Average of 1000 bootstrapped connectomes with random edge-rewiring curves in gray. Every average with 95% confidence interval. The blue bars are centered at the sample intercept filtration for starting/ending values with 95% confidence interval in dashed red. Extended Data Figure 3-1 also shows that the persistence of topological holes ( $B_1$ ) shown in B is directly related to the number of holes.

to a single component. Meanwhile, low scores of  $B_1$ -AUC mean that nodes rapidly bind to one another, fulfilling the topological holes, and higher scores imply an increase in the persistence of such holes, but also in the number of holes within the network (i.e., a less densely connected network; see Extended Data Fig. 3-1).

Furthermore, to discard that the observed results can be obtained by chance, a null distribution of Betti curves was generated by bootstrapping 1000 connectomes extracted from the original sample whose edges were randomly rewired (Giusti et al., 2015; Gracia-Tabuenca et al., 2020).

### Developmental trajectories

Developmental effects were tested using linear mixed-effects (LME) and nonlinear generalized additive mixed models (GAMM). We opted for GAMM because it allows

for testing several nonlinear trends simultaneously and can address nonparametric regression estimators (Lin et al., 2004). Additionally, given that PDS is an ordinal and not continuous variable, GAMM is a suitable modeling approach. Eight models were applied: two LME for age and age-sex interaction, six GAMM fitting smooth splines for age and age-by-sex, PDS and PDS-by-sex, and Age-PDS interaction and Age-PDS interaction-by-sex. The longitudinal dimensions of the sample were modeled by intraindividual intercepts, which accounted for the random-effects of the models, and were estimated via maximum likelihood. Additionally, every model included the average head motion (FD-RMS) and coil as confounds. Models were implemented using R libraries: LME via *lme4* (Bates et al., 2007; RRID:SCR\_015654), GAMM via *gamm4* (Wood et al., 2017). The selection of the best model was set by the lowest Akaike Information Criterion (AIC; Akaike, 1974). The AIC evals a model by the trade-off between its complexity and its goodness of fit. That is, the subtraction between the number of parameters ( $k$ ) and the log-likelihood function ( $\ln L$ ) by a factor of two (i.e.,  $AIC = 2k - 2\ln L$ ). Thus, based on information theory, the best model is the one with the minimum AIC value. Model assumptions were evaluated with Shapiro-Wilk normality tests on the residuals and random-effects (Verbeke and Lesaffre, 1996). Developmental terms within the model with lower AIC were tested via  $F$  tests (Wood, 2013).

In addition, the model with lower AIC at the whole-brain level was applied for the thirteen functional networks of the Power et al. (2011) segmentation, where their corresponding significance was corrected for multiple testing using a false discovery rate (FDR)  $q < 0.05$  (Benjamini and Hochberg, 1995).

### Code accessibility

All preprocessed data and the code described in this study are freely available online at [https://github.com/BrainMapINB/Pubertal\\_TDA](https://github.com/BrainMapINB/Pubertal_TDA). Also, the code is available as Extended Data 1. Present results were computed with an Intel Core i7-4790 CPU @ 3.60 GHz  $\times$  8 with Ubuntu 18.04.3 LTS 64-bit.

**Table 1: Akaike Information Criterion (AIC), Shapiro-Wilk test (SW) for the residuals (e) and random-effects (RE) for Betti-0 ( $B_0$ ) and Betti-1 ( $B_1$ ) areas under the curve (AUC) at every developmental model**

	$B_0$ -AUC			$B_1$ -AUC		
	AIC	e-SW(p)	RE-SW(p)	AIC	e-SW(p)	RE-SW(p)
LME-Age	863	0.993 (0.71)	0.984 (0.36)	627.6	0.98 (0.04)	0.974 (0.07)
LME-Age.Sex	864.9	0.994 (0.82)	0.984 (0.35)	631.3	0.98 (0.04)	0.974 (0.07)
GAMM-Age	861.4	0.994 (0.79)	0.987 (0.53)	627.7	0.986 (0.18)	0.981 (0.22)
GAMM-Age.Sex	862.9	0.994 (0.82)	0.986 (0.49)	630.9	0.987 (0.21)	0.981 (0.22)
GAMM-PDS	858.3	0.992 (0.65)	0.983 (0.31)	625.6	0.989 (0.36)	0.988 (0.63)
GAMM-PDS.Sex	859.5	0.991 (0.57)	0.979 (0.15)	633.1	0.985 (0.14)	0.984 (0.37)
GAMM-AgePDS	859.4	0.994 (0.82)	0.983 (0.3)	625.9	0.991 (0.54)	0.987 (0.53)
GAMM-AgePDS.Sex	862.5	0.993 (0.74)	0.983 (0.3)	631.7	0.991 (0.57)	0.979 (0.17)

Developmental models: linear mixed-effects models for age (LME-Age) and age-sex interaction (LME-Age.Sex), generalized additive mixed models with smooth splines for age (GAMM-Age) and age-by-sex (GAMM-Age.Sex), PDS (GAMM-PDS) and PDS-by-sex (GAMM-PDS.Sex), and age-PDS interaction (GAMM-AgePDS) and age-PDS interaction-by-sex (GAMM-AgePDS.Sex). Akaike Information Criterion (AIC) and Shapiro-Wilk tests (SW) for the residuals (e) and random-effects (RE) of the Betti-0 ( $B_0$ ) and Betti-1 ( $B_1$ ) areas under the curve (AUC) for every developmental model.

Concerning the developmental effects at the functional network level, the PDS term showed strong effects in the fronto-parietal (FPN) and moderate effects in the auditory (AUD), sensorimotor-hand (SMH), and subcortical (SUB) networks for the  $B_0$ -AUC (Fig. 5). Only the FPN had a significant effect after FDR correction ( $F = 6.84$ ;  $EDF = 2.09$ ;  $p = 0.001$ ), which shows a nonlinear trend similar to the whole brain network (Fig. 6). No effects (even uncorrected) were found for the  $B_1$ -AUC.

**Table 2: Model performance at the RSN, effective degrees of freedom (EDF),  $F$  and  $p$  values for the development component**

	EDF	B <sub>0</sub> -AUC		EDF	B <sub>1</sub> -AUC	
		$F$	$p$		$F$	$p$
AUD	1	0.47	0.493	1.93	1.82	0.156
CBL	1	0.04	0.838	1	1.16	0.283
CON	1.91	2.38	0.067	1	0.44	0.506
DMN	1	0.37	0.543	1	0.02	0.896
DAN	1.78	1.57	0.203	1	0.01	0.904
FPN	2.09	6.84	0.001*	1	3.21	0.076
MEM	1	0.07	0.794	1	2.03	0.157
SAL	1	4.09	0.045	1	0.82	0.368
SMH	1	2.74	0.1	1	0.04	0.839
SMM	1	1.83	0.178	1	0.26	0.611
SUB	1	1.98	0.162	1	0.24	0.628
VAN	1	0.16	0.691	1	1.12	0.291
VIS	1	3.81	0.053	1	4.01	0.047

Auditory (AUD), cerebellar (CBL), cingulo-opercular (CON), default mode (DMN), dorsal attention (DAN), fronto-parietal (FPN), memory-retrieval (MEM), salience (Sal), sensorimotor-hand (SMH), sensorimotor-mouth (SMM), subcortical (Sub), ventral attention (VAN), and visual (VIS) networks.

\* Significant after FDR-corrected at  $q < 0.05$ .

## Results

The sample intercept B<sub>0</sub> curve, the representative curve for the whole sample, showed an inverse sigmoid pattern with a slower transition to the single component compared with the permuted data (Fig. 3A), which means that the brain topology is more complex compared with a random network. On the other hand, the B<sub>1</sub> curve shows a bell shape with a maximum of 104.69 “holes” at 0.432 filtration value, while the permuted data shows a maximum of 183.92 at  $\varepsilon = 0.438$  (Fig. 3B). This implies that the brain network has a more densely connected pattern, compared with random networks, and therefore less number of topological holes.

In addition, the average filtration value where B<sub>0</sub> curves get to the value of 1 is 0.5474, with a 95% confidence interval of [0.527, 0.5677] (Fig. 3A). The average filtration value where B<sub>1</sub> curves begin to increase above 0 is 0.1627, with a 95% confidence interval of [0.1554, 0.1699]. Similarly, the average filtration value where B<sub>1</sub> curves return to 0 is 0.718, with a 95% confidence interval of [0.7118, 0.7242] (Fig. 3B). This information means that both the B<sub>0</sub> and the B<sub>1</sub> curves start and end around the same filtration values. That is, two Betti curves with similar areas will not have extremal differences in their curve profiles.

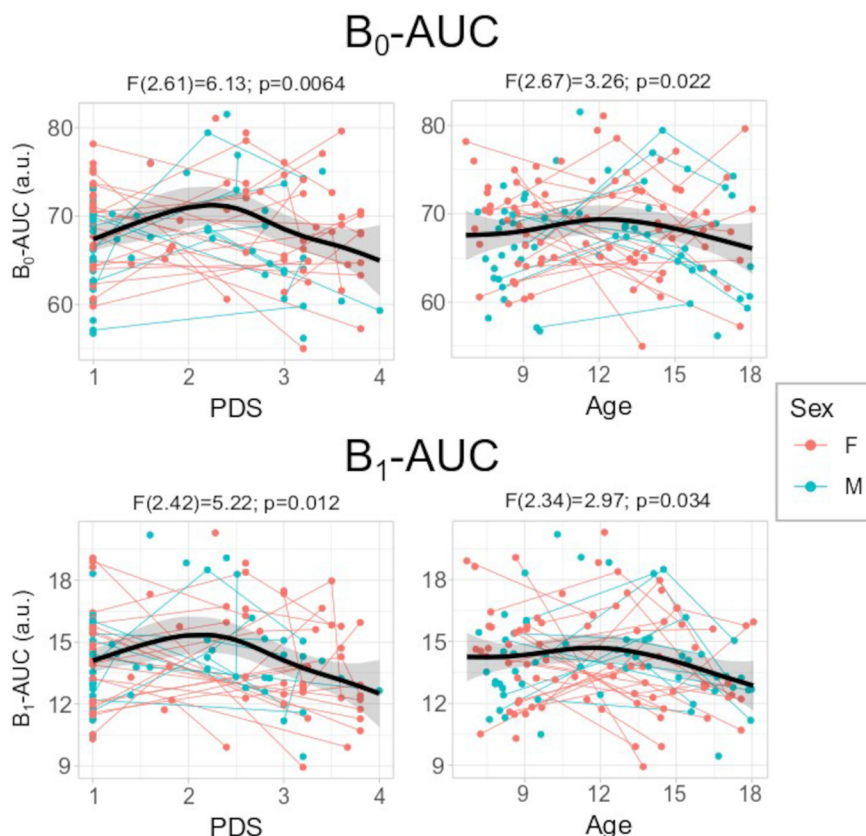


**Figure 4.** Scatter-plots of the GAMM PDS (left) and age (right) models for the B<sub>0</sub> (top) and B<sub>1</sub> (bottom) area under de curve (AUC) in relation to the pubertal scale (PDS) or age (in years). Thin lines represent individual trajectories; thick black lines represent the sample curve (with 95% confidence-interval shadow). Smooth spline  $F$  statistics are depicted. GAMM-age adjustments have higher AIC than GAM-PDS, but are depicted as a reference. a.u., arbitrary units. The relationship between the PDS or Age and the TDA features residuals after regressing out average motion, head coil, and intraindividual slopes covariates is included in Figure Extended Data Figure 4-1. F, females; M, males.

Regarding model selection for the developmental effects, the GAMM for the PDS showed the lowest AIC for  $B_0$ -AUC (858.3) and  $B_1$ -AUC (625.6; Table 1). Additionally, the normality assumption was rejected (based on the nominal  $\alpha=0.05$ ) only in the residuals of the linear mixed-models of the  $B_1$ -AUC, but the assumption remains for all of the nonlinear models as well as all  $B_0$ -AUC models tested. The  $B_0$ -AUC and  $B_1$ -AUC trends along the PDS show an initial increase from level 1 to 2, followed by a soft decline after that (Fig. 4). Both effects were significant ( $B_0$ -AUC:  $F=6.13$ ,  $EDF=2.61$ ,  $p=0.0064$ ;  $B_1$ -AUC:  $F=5.22$ ,  $EDF=2.42$ ,  $p=0.012$ ).

## Discussion

In this study, we have applied Topological Data Analysis (TDA) on the functional connectomes of a longitudinal sample of typically developing children and adolescents. TDA features show a more distributed connectivity structure compared with random networks. However, when assessing the connectivity structure within the connected nodes, the brain connectomes exhibit a more densely connected pattern than the random networks. Furthermore, this topology develops nonlinearly through adolescence, better adjusted to pubertal status than chronological age. This nonlinear effect exhibits a stronger connectivity of the whole-network and within the fronto-parietal network just after the onset of the pubertal signs.

Regarding the average Betti curves, the sample intercept for the  $B_0$  curve showed an inverse sigmoid pattern that replicates previous findings in functional connectivity fMRI (Liang and Wang, 2017; Gracia-Tabuenca et al., 2020; Li et al., 2021) and PET (H. Lee et al., 2012) studies. Furthermore, the average  $B_0$  curve of the randomized data reached the single component faster than the observed data, evincing a less distributed network. This random pattern was also replicated in another pediatric sample showing the same faster transition to a single component (Gracia-Tabuenca et al., 2020). Concerning the  $B_1$ , both the sample intercept and randomized curves exhibit a bell-shaped curve with an approximately similar filtration value at their maxima but at a lower area for the observed data. This information evinces a connectivity topology structure of a lower number of holes or more densely connected at the local level in the real data compared with the random networks. Thus,  $B_0$  tells how fast the whole-network goes from isolated to all-connected nodes, while  $B_1$  reflects how densely connected those elements are already connected. It is noticeable that, on average,  $B_0$  tends to reach the single component at filtration values of  $\varepsilon = 0.5$ , but at that point,  $B_1$  curves display their peak number of “holes.” This information implies that these TDA features not only reflect different levels of connectivity structure but also occur at different connectivity strengths.

Regarding the developmental effects of the TDA features, several models were tested to address the area under the  $B_0$  and  $B_1$  curves. Nonlinear additive models show greater goodness of fit compared with linear ones, even controlling for the extra number of parameters. Specifically, when considering the pubertal status (assessed by the PDS) without its sex interaction is the

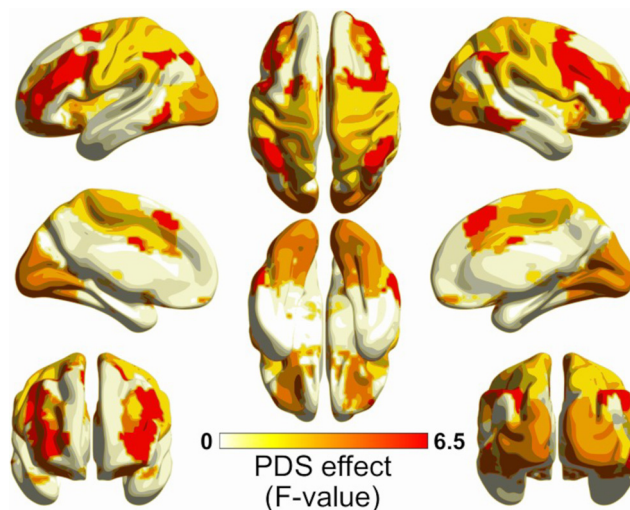


**Figure 5.** Brain maps of the smooth spline's  $F$  value of the Pubertal Development Scale (PDS) GAMM term for  $B_0$ -AUC at the functional networks level. Mapping was based on ROI corresponding to the consensus area according to Power et al. (2011), using BrainNet Viewer (Xia et al., 2013; RRID:SCR\_009446).

model that better fits the AUC for both  $B_0$  and  $B_1$ . Hence, the development of the functional connectome topology better adjusts pubertal status than chronological age. This is a relevant finding considering that the pubertal status takes into account noncontinuous changes as well as more subtle sex effects than a nonlinear age-sex interaction. No previous studies have addressed the adolescent connectome via TDA, but recent studies have

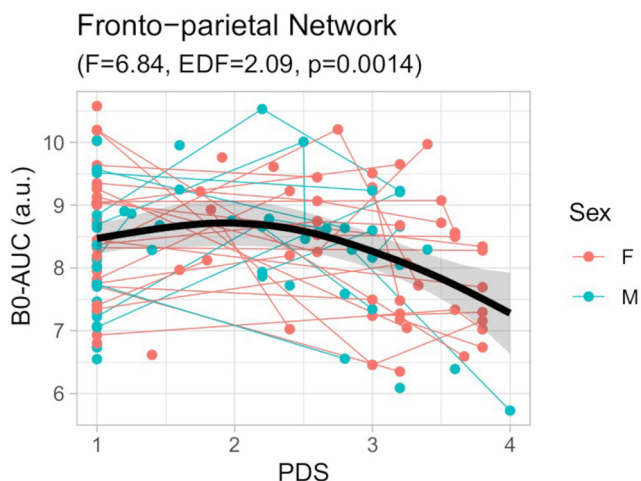


**Figure 6.** Scatter-plot of the GAMM model for the  $B_0$ -AUC of the fronto-parietal network (FPN) in relation to the pubertal scale (PDS). Thin lines represent individual trajectories; thick black lines represent the sample's smooth spline curve (with 95% confidence-interval shadow). Smooth spline  $F$  statistics are depicted. a.u., arbitrary units. The relationship between the PDS and the  $B_0$ -AUC residuals after regressing out average motion, head coil, and intraindividual slopes covariates is included in Extended Data Figure 6-1. EDF, effective degrees of freedom.



shown a better adjustment with the pubertal status for the developmental trends of the functional connectome (based on graph theory; Gracia-Tabuenca et al., 2021) or the fronto-triatrial functional connectivity (van Duijvenvoorde et al., 2019). Previous studies in animal models have shown brain plasticity associated with puberty-related hormonal changes (Sisk and Foster, 2004). Neuroimaging studies controlling for the age effects have also revealed structural changes associated with the puberty stage in humans, mainly showing decreased gray matter density but increased white matter density in later stages (Peper et al., 2009; Perrin et al., 2009; Bramen et al., 2011; Herting et al., 2012). This work contributes to the emerging evidence that puberty onset dramatically influences the development of functional brain connectivity (van Duijvenvoorde et al., 2019; Gracia-Tabuenca et al., 2021).

Concerning whole-brain inferences, the AUC for both  $B_0$  and  $B_1$  showed an initial increase from PDS level 1 to 2, but decreased afterward. In contrast, when focusing on the chronological age, the turning point is  $\sim 12$  years old, but showing smoother trends compared with PDS. This means a faster transition to the single component for the  $B_0$  while a lower rate of geometric holes for the  $B_1$  at the end of adolescence when considering PDS or age. But only  $B_0$ -AUC effects were significant, which evinces that those changes were more prominent at lower filtration values, i.e., edges with higher functional connectivity (see Materials and Methods, Topological data analysis). Previous work on brain functional organization during this period has shown increases along age in the within-network connectivity (Fair et al., 2009; Satterthwaite et al., 2013a; Gu et al., 2015), while others failed to replicate that pattern showing an increase in the between-network functional connectivity instead (Hwang et al., 2013; Marek et al., 2015). In addition, when considering the PDS, it has been shown that functional centrality, segregation, efficiency, and integration increase at the end of adolescence (Gracia-Tabuenca et al., 2021). Such divergent results in neurotypical samples can be explained by the use of different samples and methods, such as selection of regions/networks of interest, thresholding, and/or connectome features. However, the present study uses longitudinal nonlinear modeling with features from the TDA framework, which is resilient thresholding and can extract high-order patterns at the local and global levels at the same time. All these studies demonstrate the change in the configuration of the brain's functional organization during adolescence.

Likewise, the  $B_0$ -AUC along the PDS effect was stronger in the Fronto-Parietal Network (FPN), showing a similar nonlinear trend as that for the whole brain network (Table 2; Figs. 5 and 6). This demonstrates a faster binding of the FPN nodes at the end of adolescence in terms of functional connectivity. The FPN is a key module of the connectome that is involved in the response to high-demanding tasks (Zanto and Gazzaley, 2013) and is a fundamental system for the consolidation of executive behavior in the adolescent period (Baum et al., 2017; Chai et al., 2017). Other works on functional connectomes have reported an increase in the FPN connectivity along with other attention-related systems in late adolescence (Hwang et al., 2013; Marek et al., 2015). In fact, when

applying the graph theory measures to this sample (in a previous study from our group, Gracia-Tabuenca et al., 2021), we found diverse connectome changes in several functional networks, including attention-related but also primary and subcortical, but when using TDA features the central role of the FPN is clearly stated among the other networks.

Some limitations of this work should be taken into account. We used relatively short scans, which may affect the quality of the data; nonetheless, it was considered sufficient at the time of the first acquisition (Van Dijk et al., 2010). Furthermore, we applied a strident quality control of the data discarding those datasets with  $< 80\%$  good quality data in terms of motion artifact. Nonetheless, Topological Data Analysis (TDA) complements other network modeling strategies by extracting high-dimensional features across the whole range of connectivity values, instead of exploring a fixed set of connections.

In conclusion, the present study focused on the characterization of functional connectomes as topological spaces in a longitudinal sample of typically developing children and adolescents. Observed Topological Data Analysis (TDA) features showed a more distributed structure but with denser local connections compared with random networks. However, during adolescence, this effect changes with a nonlinear trend for the whole-brain and the fronto-parietal network, particularly after the onset of the pubertal signs. These results provide evidence of the nonlinear, puberty-dependent developmental trajectories of the topology of the brain network. With the advantage that these properties arise when exploring the whole range of connectivity strengths instead of focusing on a small set of them. Although, as far as we are concerned, this is the first implementation of TDA into neurotypical development, we have shown that this approach can handle complex data in a multi-session design and effectively detect meaningful changes in the adolescent functional connectome. Being adolescence a critical period for the appearance of the first signs of mental health disorders, we expect these trajectories may be of interest for studying both normal and altered development.

## References

- Akaike H (1974) A new look at the statistical model identification. *IEEE Trans Automat Contr* 19:716–723.
- Avants BB, Epstein CL, Grossman M, Gee JC (2008) Symmetric diffeomorphic image registration with cross-correlation: evaluating automated labeling of elderly and neurodegenerative brain. *Med Image Anal* 12:26–41.
- Bates D, Sarkar D, Bates MD, Matrix L (2007) The lme4 package. R package version 2:74. Available at <https://CRAN.R-project.org/package=lme4>.
- Baum GL, Ciric R, Roalf DR, Betzel RF, Moore TM, Shinohara RT, Kahn AE, Vandekar SN, Rupert PE, Quarmley M, Cook PA, Elliott MA, Ruparel K, Gur RE, Gur RC, Bassett DS, Satterthwaite TD (2017) Modular segregation of structural brain networks supports the development of executive function in youth. *Curr Biol* 27:1561–1572.e8.
- Benjamini Y, Hochberg Y (1995) Controlling the false discovery rate: a practical and powerful approach to multiple testing. *J R Stat Soc Series B Stat Methodol* 57:289–300.



- Biswal B, Yetkin FZ, Haughton VM, Hyde JS (1995) Functional connectivity in the motor cortex of resting human brain using echo-planar MRI. *Magn Reson Med* 34:537–541.
- Blakemore S-J, Burnett S, Dahl RE (2010) The role of puberty in the developing adolescent brain. *Human Brain Mapping* 31:926–933.
- Bramen JE, Hranilovich JA, Dahl RE, Forbes EE, Chen J, Toga AW, Dinov ID, Worthman CM, Sowell ER (2011) Puberty influences medial temporal lobe and cortical gray matter maturation differently in boys than girls matched for sexual maturity. *Cereb Cortex* 21:636–646.
- Caputi L, Pidnebesna A, Hlinka J (2021) Promises and pitfalls of topological data analysis for brain connectivity analysis. *Neuroimage* 238:118245.
- Centeno EGZ, Moreni G, Vriend C, Douw L, Santos FAN (2022) A hands-on tutorial on network and topological neuroscience. *Brain Struct Funct* 227:741–762.
- Chai LR, Khambhati AN, Ciric R, Moore TM, Gur RC, Gur RE, Satterthwaite TD, Bassett DS (2017) Evolution of brain network dynamics in neurodevelopment. *Netw Neurosci* 1:14–30.
- Choi H, Kim YK, Kang H, Lee H, Im H-J, Hwang DW, Kim EE, Chung JK, Lee DS (2014) Abnormal metabolic connectivity in the pilocarpine-induced epilepsy rat model: a multiscale network analysis based on persistent homology. *Neuroimage* 99:226–236.
- Chung MK, Bubenik P, Kim PT (2009) Persistence diagrams of cortical surface data. *Inf Process Med Imaging* 21:386–397.
- Chung MK, Huang SG, Gritsenko A, Shen L, Lee H (2019) Statistical inference on the number of cycles in brain networks. *Proc IEEE Int Symp Biomed Imaging* 2019:113–116.
- Ciric R, Wolf DH, Power JD, Roalf DR, Baum GL, Ruparel K, Shinohara RT, Elliott MA, Eickhoff SB, Davatzikos C, Gur RC, Gur RE, Bassett DS, Satterthwaite TD (2017) Benchmarking of participant-level confound regression strategies for the control of motion artifact in studies of functional connectivity. *Neuroimage* 154:174–187.
- Cohen-Steiner D, Edelsbrunner H, Harer J, Mileyko Y (2010) Lipschitz functions have LP-stable persistence. *Found Comput Math* 10:127–139.
- Edelsbrunner H, Harer J (2010) Computational topology: An introduction. American Mathematical Soc. Available at <https://bookstore.ams.org/view?ProductCode=MBK/69>.
- Expert P, Lord LD, Kringelbach ML, Petri G (2019) Editorial: topological neuroscience. *Netw Neurosci* 3:653–655.
- Fair DA, Cohen AL, Power JD, Dosenbach NUF, Church JA, Miezin FM, Schlaggar BL, Petersen SE (2009) Functional brain networks develop from a “local to distributed” organization. *PLoS Comput Biol* 5:e1000381.
- Fasy BT, Kim J, Lecci F, Maria C (2014) Introduction to the R package TDA. arXiv 1411.1830. <https://doi.org/10.48550/arXiv.1411.1830>.
- Fonov V, Evans AC, Botteron K, Almlí CR, McKinstry RC, Collins DL; Brain Development Cooperative Group (2011) Unbiased average age-appropriate atlases for pediatric studies. *Neuroimage* 54:313–327.
- Fülöp T, Desroches M, Cohen AA, Santos FAN, Rodrigues S (2020) Why we should use topological data analysis in ageing: towards defining the “topological shape of ageing.” *Mech Ageing Dev* 192:111390.
- Garrison KA, Scheinost D, Finn ES, Shen X, Constable RT (2015) The (in) stability of functional brain network measures across thresholds. *Neuroimage* 118:651–661.
- Giusti C, Pastalkova E, Curto C, Itskov V (2015) Clique topology reveals intrinsic geometric structure in neural correlations. *Proc Natl Acad Sci U S A* 112:13455–13460.
- Gracia-Tabuenca Z, Díaz-Patiño JC, Arelio I, Alcauter S (2020) Topological data analysis reveals robust alterations in the whole-brain and frontal lobe functional connectomes in attention-deficit/hyperactivity disorder. *eNeuro* 7:ENEURO.0543-19.2020.
- Gracia-Tabuenca Z, Moreno MB, Barrios FA, Alcauter S (2021) Development of the brain functional connectome follows puberty-dependent nonlinear trajectories. *Neuroimage* 229:117769.
- Graff K, Tansey R, Ip A, Rohr C, Dimond D, Dewey D, Bray S (2022) Benchmarking common preprocessing strategies in early childhood functional connectivity and intersubject correlation fMRI. *Dev Cogn Neurosci* 54:101087.
- Gu S, Satterthwaite TD, Medaglia JD, Yang M, Gur RE, Gur RC, Bassett DS (2015) Emergence of system roles in normative neurodevelopment. *Proc Natl Acad Sci U S A* 112:13681–13686.
- Herting MM, Maxwell EC, Irvine C, Nagel BJ (2012) The impact of sex, puberty, and hormones on white matter microstructure in adolescents. *Cereb Cortex* 22:1979–1992.
- Hibberd EE, Hackney AC, Lane AR, Myers JB (2015) Assessing biological maturity: chronological age and the pubertal development scale predict free testosterone in adolescent males. *J Pediatr Endocrinol Metab* 28:381–386.
- Hwang K, Hallquist MN, Luna B (2013) The development of hub architecture in the human functional brain network. *Cereb Cortex* 23:2380–2393.
- Jenkinson M, Bannister P, Brady M, Smith S (2002) Improved optimization for the robust and accurate linear registration and motion correction of brain images. *Neuroimage* 17:825–841.
- Jenkinson M, Beckmann CF, Behrens TE, Woolrich MW, Smith SM (2012) FSL. *Neuroimage* 62:782–790.
- Laube C, van den Bos W, Fandakova Y (2020) The relationship between pubertal hormones and brain plasticity: implications for cognitive training in adolescence. *Dev Cogn Neurosci* 42:100753.
- Lee H, Chung MK, Kang H, Kim BN, Lee DS (2011) Discriminative persistent homology of brain networks. 2011 IEEE international symposium on biomedical imaging: from nano to macro, pp 841–844, Chicago, IEEE.
- Lee H, Kang H, Chung MK, Kim BN, Lee DS (2012) Persistent brain network homology from the perspective of dendrogram. *IEEE Trans Med Imaging* 31:2267–2277.
- Lee H, Kang H, Chung MK, Lim S, Kim BN, Lee DS (2017) Integrated multimodal network approach to PET and MRI based on multidimensional persistent homology. *Hum Brain Mapp* 38:1387–1402.
- Lee H, Chung MK, Kang H, Choi H, Ha S, Huh Y (2019) Coidentification of group-level hole structures in brain networks via Hodge Laplacian. In: *Medical Image Computing and Computer Assisted Intervention – MICCAI 2019 Lecture Notes in Computer Science* (Shen D, Liu T, Peters TM, Staib LH, Essert C, and Zhou S, eds). Cham: Springer International Publishing.
- Lee MH, Kim DY, Lee SH, Kim JU, Chung MK (2015) Comparisons of topological properties in autism for the brain network construction methods. In: *Medical imaging 2015: image processing (SPIE)*, pp 559–564. SPIE Medical Imaging, 2015, Orlando, Florida, United States. SPIE.
- Li J, Bian C, Luo H, Chen D, Cao L, Liang H (2021) Multi-dimensional persistent feature analysis identifies connectivity patterns of resting-state brain networks in Alzheimer’s disease. *J Neural Eng*. Advance online publication. Retrieved Feb 16, 2021. <https://doi.org/10.1088/1741-2552/abc7ef>.
- Liang H, Wang H (2017) Structure-function network mapping and its assessment via persistent homology. *PLoS Comput Biol* 13:e1005325.
- Lin X, Wang N, Welsh AH, Carroll RJ (2004) Equivalent kernels of smoothing splines in nonparametric regression for clustered/longitudinal data. *Biometrika* 91:177–193.
- Lord LD, Expert P, Fernandes HM, Petri G, Van Hartevelt TJ, Vaccarino F, Deco G, Turkheimer F, Kringelbach ML (2016) Insights into brain architectures from the homological scaffolds of functional connectivity networks. *Front Syst Neurosci* 10:85.
- Manjón JV, Coupé P, Martí-Bonmatí L, Collins DL, Robles M (2010) Adaptive non-local means denoising of MR images with spatially varying noise levels. *J Magn Reson Imaging* 31:192–203.
- Marek S, Hwang K, Foran W, Hallquist MN, Luna B (2015) The contribution of network organization and integration to the development of cognitive control. *PLoS Biol* 13:e1002328.

- Parkes L, Fulcher B, Yücel M, Fornito A (2018) An evaluation of the efficacy, reliability, and sensitivity of motion correction strategies for resting-state functional MRI. *Neuroimage* 171:415–436.
- Peper JS, Schnack HG, Brouwer RM, Van Baal GCM, Pjetri E, Székely E, van Leeuwen M, van den Berg SM, Collins DL, Evans AC, Boomsma DI, Kahn RS, Hulshoff Pol HE (2009) Heritability of regional and global brain structure at the onset of puberty: a magnetic resonance imaging study in 9-year-old twin pairs. *Hum Brain Mapp* 30:2184–2196.
- Perrin JS, Leonard G, Perron M, Pike GB, Pitiot A, Richer L, Veillette S, Pausova Z, Paus T (2009) Sex differences in the growth of white matter during adolescence. *Neuroimage* 45:1055–1066.
- Petersen AC, Crockett L, Richards M, Boxer A (1988) A self-report measure of pubertal status: reliability, validity, and initial norms. *J Youth Adolesc* 17:117–133.
- Power JD, Cohen AL, Nelson SM, Wig GS, Barnes KA, Church JA, Vogel AC, Laumann TO, Miezin FM, Schlaggar BL, Petersen SE (2011) Functional network organization of the human brain. *Neuron* 72:665–678.
- Rubinov M, Sporns O (2010) Complex network measures of brain connectivity: uses and interpretations. *Neuroimage* 52:1059–1069.
- Rieck B, Sadlo F, Leitte H (2020) Topological machine learning with persistence indicator functions. In: *Topological methods in data analysis and visualization V. Mathematics and visualization* (Carr H, Fujishiro I, Sadlo F, and Takahashi S, eds), pp 87–101. Cham: Springer International Publishing.
- Santos FA, Raposo EP, Coutinho-Filho MD, Copelli M, Stam CJ, Douw L (2019) Topological phase transitions in functional brain networks. *Phys Rev E* 100:e032414.
- Satterthwaite TD, Wolf DH, Loughhead J, Ruparel K, Elliott MA, Hakonarson H, Gur RC, Gur RE (2012) Impact of in-scanner head motion on multiple measures of functional connectivity: relevance for studies of neurodevelopment in youth. *Neuroimage* 60:623–632.
- Satterthwaite TD, Wolf DH, Ruparel K, Erus G, Elliott MA, Eickhoff SB, Gennatas ED, Jackson C, Prabhakaran K, Smith A, Hakonarson H, Verma R, Davatzikos C, Gur RE, Gur RC (2013a) Heterogeneous impact of motion on fundamental patterns of developmental changes in functional connectivity during youth. *Neuroimage* 83:45–57.
- Satterthwaite TD, Elliott MA, Gerraty RT, Ruparel K, Loughhead J, Calkins ME, Eickhoff SB, Hakonarson H, Gur RC, Gur RE, Wolf DH (2013b) An improved framework for confound regression and filtering for control of motion artifact in the preprocessing of resting-state functional connectivity data. *Neuroimage* 64:240–256.
- Sawyer SM, Azzopardi PS, Wickremarathne D, Patton GC (2018) The age of adolescence. *Lancet Child Adolesc Health* 2:223–228.
- Sisk CL, Foster DL (2004) The neural basis of puberty and adolescence. *Nat Neurosci* 7:1040–1047.
- Sizemore AE, Giusti C, Kahn A, Vettel JM, Betzel RF, Bassett DS (2018) Cliques and cavities in the human connectome. *J Comput Neurosci* 44:115–145.
- Sizemore AE, Phillips-Cremins JE, Ghrist R, Bassett DS (2019) The importance of the whole: topological data analysis for the network neuroscientist. *Netw Neurosci* 3:656–673.
- Smith SM, Fox PT, Miller KL, Glahn DC, Fox PM, Mackay CE, Filippini N, Watkins KE, Toro R, Laird AR, Beckmann CF (2009) Correspondence of the brain's functional architecture during activation and rest. *Proc Natl Acad Sci U S A* 106:13040–13045.
- Taymourtash A, Schwartz E, Nenning KH, Sobotka D, Diogo M, Kasprian G, Prayer D, Langs G (2019) Quantifying residual motion artifacts in fetal fMRI data. In: *Smart ultrasound imaging and perinatal, preterm and paediatric image analysis*, pp 171–180. Cham: Springer.
- Tustison NJ, Avants BB, Cook PA, Zheng Y, Egan A, Yushkevich PA, Gee JC (2010) N4ITK: improved N3 bias correction. *IEEE Trans Med Imaging* 29:1310–1320.
- Van Dijk KR, Hedden T, Venkataraman A, Evans KC, Lazar SW, Buckner RL (2010) Intrinsic functional connectivity as a tool for human connectomics: theory, properties, and optimization. *J Neurophysiol* 103:297–321.
- van Duijvenvoorde ACK, Westhoff B, de Vos F, Wierenga LM, Crone EA (2019) A three-wave longitudinal study of subcortical–cortical resting-state connectivity in adolescence: testing age- and puberty-related changes. *Hum Brain Mapp* 40:3769–3783.
- Verbeke G, Lesaffre E (1996) A linear mixed-effects model with heterogeneity in the random-effects population. *J Am Stat Assoc* 91:217–221.
- Vijayakumar N, de Macks ZO, Shirtcliff EA, Pfeifer JH (2018) Puberty and the human brain: insights into adolescent development. *Neurosci Biobehav Rev* 92:417–436.
- Wood SN (2013) On p-values for smooth components of an extended generalized additive model. *Biometrika* 100:221–228.
- Wood S, Scheipl F, Wood MS (2017) Package 'gamm4.' *Am Stat* 45:339. Available at <https://CRAN.R-project.org/package=gamm4>.
- Xia M, Wang J, He Y (2013) BrainNet Viewer: a network visualization tool for human brain connectomics. *PLoS One* 8:e68910.
- Zanto TP, Gazzaley A (2013) Fronto-parietal network: flexible hub of cognitive control. *Trends Cogn Sci* 17:602–603.